Available online at www.sciencedirect.com

ScienceDirect

Procedia CIRP 143 (2026) 183–189

www.elsevier.com/locate/procedia

14th CIRP Conference on Photonic Technologies

Synchrotron X-ray imaging of the formation of transverse hot cracks during laser welding of a high-strength aluminum alloy and their dependence on local solidification conditions and process parameters

Johannes Michel[a,*], Michael Haas[a,b], Robert Steinhoff[a], Michael Sawannia[a], Christoph Spurk[c], Marc Hummel[c,d], Alexander Olowinsky[d], Felix Beckmann[e], Julian Moosmann[e], Christian Hagenlocher[a], Thomas Graf[a]

[a]*Institut für Strahlwerkzeuge (IFSW), University of Stuttgart, Pfaffenwaldring 43, 70569 Stuttgart, Germany*
[b]*Graduate School of Excellence advanced Manufacturing Engineering (GSaME), University of Stuttgart, Nobelstr. 12, 70569 Stuttgart, Germany*
[c]*RWTH Aachen University, Chair for Laser Technology LLT, Steinbachstraße 15, 52074 Aachen, Germany*
[d]*Fraunhofer Institute for Laser Technology ILT, Steinbachstraße 15, 52074 Aachen, Germany*
[e]*Institute of Materials Physics, Helmholtz-Zentrum Hereon, Max-Planck-Str. 1, 21502 Geesthacht, Germany*

* Corresponding author. Tel.: +49 711 685-60428, *E-mail address:* johannes.michel@ifsw.uni-stuttgart.de

Abstract

The formation of transverse hot cracks in the weld seam limits the use of laser welding for high-strength aluminum alloys in lightweight electromobility applications. While transverse hot cracks initiate in the semisolid region, their exact location relative to the melt pool boundary and their relation to local solidification conditions and process parameters remain unclear. In this study, the formation of transverse hot cracks was investigated using in-situ synchrotron X-ray imaging. Crack initiation and propagation relative to the melt pool boundary, crack propagation rates, solidification rates, and the number of transverse cracks in the weld seam were evaluated as a function of welding speed and laser power. The results show that the average crack propagation rate corresponds to the local solidification rate along the melt pool boundary encountered during propagation. Increasing welding speed at constant weld depth increased both the crack propagation rate and the number of cracks in the weld seam. Reduced laser power at a constant welding speed resulted in higher crack propagation rates and more, but shallower, cracks. The findings advance the understanding of the mechanisms underlying transverse hot cracking and provide a basis for developing mitigation strategies.

© 2026 The Authors. Published by Elsevier B.V.
This is an open access article under the CC BY license (http://creativecommons.org/licenses/by/4.0/)
Peer-review under responsibility of the scientific committee of the 14th CIRP Conference on Photonic Technologies [LANE 2026]

Keywords: Laser welding; Transverse hot cracks; Synchrotron X-Ray imaging; Aluminum alloys; Solidification

1. Introduction

The formation of transverse hot cracks in the weld seam during solidification limits the use of laser welding of high-strength aluminum alloys for electromobility applications [1], as cracks can lead to leakage of the coolant. Although the mechanisms of transverse hot cracking have been addressed in the literature [1–4] and strategies to mitigate transverse hot cracks, such as preheating [2] or using samples with residual compressive stresses [5], have been proposed, transverse hot cracking remains a major challenge. Real-time observation of the mechanisms underlying the formation of transverse hot cracks by synchrotron X-ray imaging provides insights to guide strategies to reduce hot cracking. Previous studies using synchrotron X-ray imaging of hot cracks during laser welding of aluminum alloys have addressed end-crater cracking in

2212-8271 © 2026 The Authors. Published by Elsevier B.V.
This is an open access article under the CC BY license (http://creativecommons.org/licenses/by/4.0/)
Peer-review under responsibility of the scientific committee of the 14th CIRP Conference on Photonic Technologies [LANE 2026]
10.1016/j.procir.2026.07.040

AA7075 [6], the influence of the local solidification conditions during pulsed laser welding [7], and hot crack formation during laser additive manufacturing [8–10]. Nevertheless, the position of transverse hot crack initiation and propagation relative to the melt pool boundary and their dependence on local solidification conditions and the process parameters during laser welding is unclear. Therefore, the influence of process parameters on transverse hot cracking during laser welding was analyzed using in-situ synchrotron X-ray imaging.

2. Experimental Setup

The X-ray imaging system at the beamline P07 (EH4) operated by Helmholtz-Zentrum Hereon at PETRA III (DESY, Hamburg, Germany) [11] was used to investigate transverse hot cracking during laser welding in a high-strength aluminum alloy. Fig. 1 shows a schematic of the experimental setup. Samples of the aluminum alloy s650 from Novelis containing 0.7 wt.% Si and 0.9 wt.% Mg [1, 12] were used. The samples had dimensions of 100 mm × 30 mm × 3 mm. The X-ray beam, with a photon energy of 37 keV, illuminated a field of 2.8 × 2.0 mm^2 located in the center of the sample along the welding direction. The converted visible light from the 1.6 mm thick GaGG: Ce scintillator was recorded using a high-speed camera (i-SPEED 727 from iX Cameras) operating at a framerate of 18298 Hz and a resolution of 2.55 µm/pixel.

A TruDisk 8001 laser from TRUMPF, which provides a laser beam with a wavelength of 1030 nm, was used. The beam was transmitted by a ring-core fiber (BrightLine Weld) with a core diameter of 100 µm and a ring diameter of 400 µm. 70 % of the laser power P was guided in the core fiber and 30 % in the ring fiber. A galvanometer scanner optic was used to move the laser beam in positive x_w-direction over the surface of the static sample, enabling the observation of the formation of transverse hot cracks in the semisolid region. The scanner optics included a collimation lens with a focal length of 80 mm and a focusing lens with a focal length of 163 mm, resulting in an optical magnification of 2.04 and a focal diameter of the core beam of 204 µm and 815 µm of the ring beam on the surface of the sample. 70 mm long weld seams were produced. A crossjet with compressed air was used to protect the optics.

The influence of the laser power P was investigated at a welding speed of v = 30 m/min, using laser powers of P = 3500, 4000, 4700, 5700 W. Additionally, the influence of welding speeds of v = 6, 12, 18, 30 m/min were evaluated at a weld depth of s = 1.5 mm with corresponding laser powers of P = 1900, 2600, 3600, 5700 W.

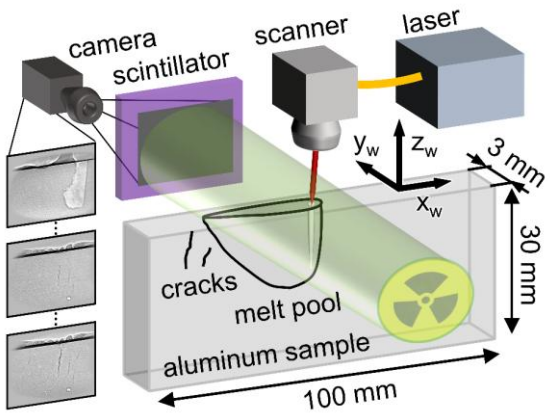


Fig. 1. Schematic of experimental setup.

3. Quantitative analysis of transverse hot cracks

Post-process X-ray scans of the welded samples were acquired to quantify the number of transverse hot cracks in the weld seam. Fig. 2 presents 20 mm long parts of the X-ray scans in a longitudinal view. The black rectangle highlights the part of the weld seam corresponding to the image field of the in-situ X-ray recordings (see Fig. 4). Fig. 2a-d show X-ray scans of the welds produced at a welding speed of v = 30 m/min with laser powers of P = 3500, 4000, 4700, and 5700 W, resulting in weld depths of s = 0.75, 1.0, 1.25, and 1.5 mm, respectively. An increase in the laser power P results in a decrease in the number of cracks per centimeter of the weld seam and an increase in the height of the transverse hot cracks.

Fig. 2d-g illustrate that the number of transverse hot cracks in the weld seam increases with increasing welding speed, which is consistent with observations in previous work [1]. In the experiments presented here, almost all transverse hot cracks at welding speeds below 12 m/min were initiated at pores.

Fig. 3 compares the average number of transverse hot cracks of three weld seams, determined from the central 50 mm of the 70 mm long X-ray scans. The minimum and maximum error bars span the minimum and maximum measured number of transverse hot cracks over three samples welded with the same process parameters. The number of transverse hot cracks decreases with increasing laser powers P at the investigated welding speed of 30 m/min (Fig. 3a), and increases with increasing welding speed at a weld depth of s = 1.5 mm (Fig. 3b).

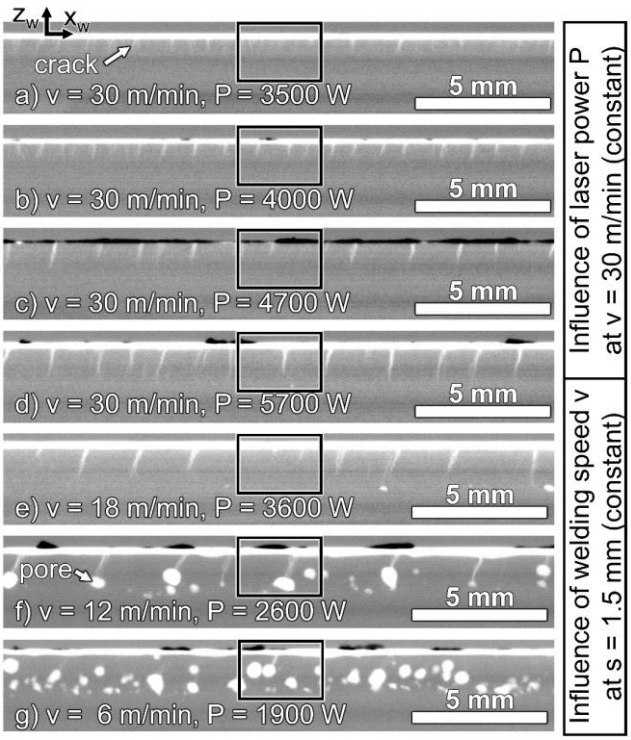


Fig. 2. X-ray scans of the weld seam in a longitudinal view. (a-d) Welds produced at a welding speed of v = 30 m/min and different laser powers P. (d-g) Welds produced at welding speeds of v = 30 m/min (d), v = 18 m/min (e), v = 12 m/min (f), and v = 6 m/min (g), with the laser power P adjusted for a weld depth of s = 1.5 mm.

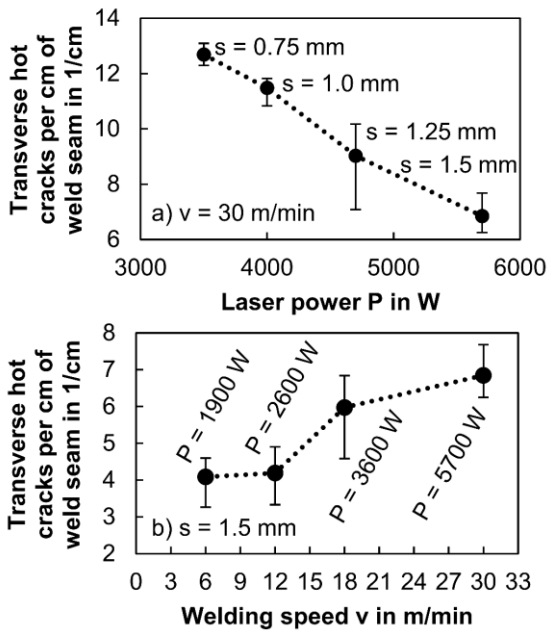


Fig. 3. Number of transverse hot cracks per unit of weld seam length as a function of the laser power P at a welding speed of v =30 m/min (a) and the welding speed v at a weld depth of s = 1.5 mm (b).

4. Analysis of crack propagation and solidification rates

Fig. 4 shows an image sequence of a flat field-corrected in-situ X-ray recording for a weld with a welding speed of v = 30 m/min and a laser power P = 5700 W. Fig. 4a shows a single image recorded at t = 69.68 ms after the start of the weld, when the vapor capillary has reached the right side of the image field. The melt pool boundary between the liquid and the semisolid region appears as a dark line in the X-ray recording (Fig. 4a). In the subsequent images, the melt pool boundary is highlighted by a blue-dashed line. At $t = t_{init}$ = 80.50 ms (Fig. 4c), a transverse hot crack is initiated in the semisolid region below the melt pool, appearing as a dark line. The transverse crack further propagates (Fig. 4d) until it stops after $t = t_{stop}$ = 88.21 ms at the surface of the sample (Fig. 4e).

To evaluate the influence of the process parameters on the initiation and propagation of transverse cracks, the x-position of crack initiation, x_{init} (Fig. 4c), the position where the transverse cracks stop or reach the surface of the sample, x_{stop} (Fig. 4e), and the position of the end of the melt pool, x_{end} (Fig. 4d), were determined. The positions were defined relative to the center of the moving capillary at x = 0 mm.

Streak images were processed from the X-ray recordings to visualize the formation of transverse hot cracks and their position relative to the melt pool boundary in a stationary condition in a single image. Fig. 5a shows one representative streak image, corresponding to the position marked by the orange vertical line in Fig. 4f. The streak images were scaled in the x-direction with respect to the welding speed and the framerate, correcting each pixel column of the streak image to represent the correct spatial dimensions.

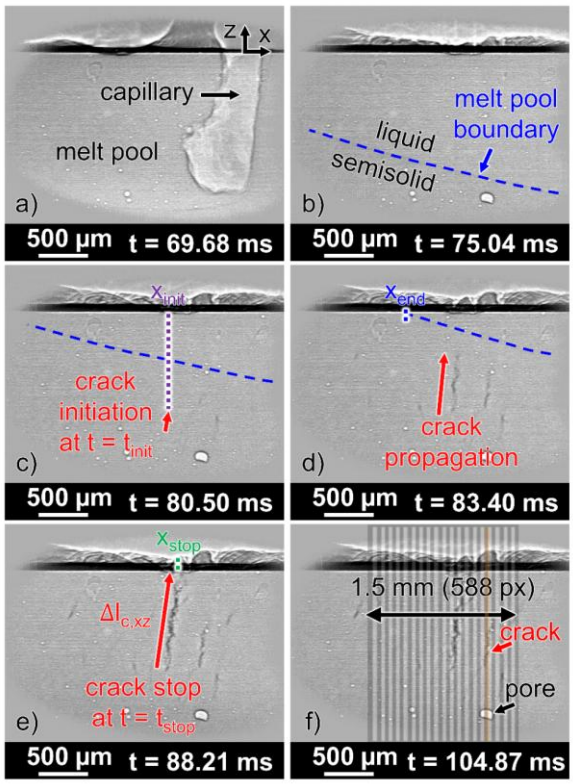


Fig. 4. X-ray image sequence during welding with v = 30 m/min and P = 5700 W showing the capillary (a); the melt pool with the boundary between the liquid and semisolid region (b); the initiation of transverse hot cracks (c); the propagation of cracks (d); and the stop of the cracks at the surface of the sample (e), as well as an image after the weld with a schematic of the image processing method (f). The video file is available at [13].

To analyze the entire width of the cracks and the position of multiple transverse hot cracks and to obtain a more realistic representation of the melt pool boundary and capillary, multiple streak images were processed. The streak images correspond to 588 pixel columns (vertical lines in Fig. 4f) spanning a width of 1.5 mm in the X-ray recording. The streak images were aligned according to their x-position in the image field to compensate for the varying column positions at which they were generated.

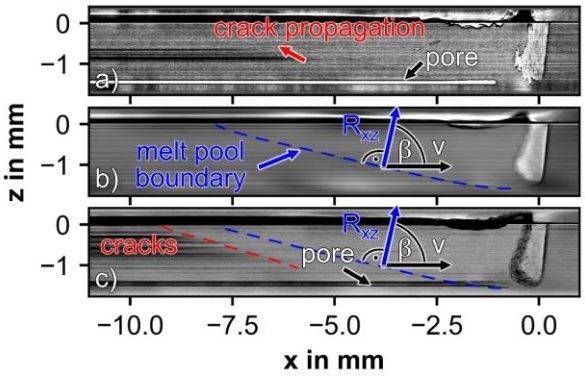


Fig. 5. Single streak image from X-ray recording (a); average (b) and minimum (c) image projection of the aligned stack of streak images for a weld with a welding speed of v = 30 m/min and a laser power of P = 5700 W.

The streak images were referenced to the center of the moving capillary at x = 0 mm. Fig. 5b-c show the average (Fig. 5b) and minimum (Fig. 5c) intensity projections computed from the aligned stack of streak images. The projections show a static time-averaged representation of the capillary, the melt pool, and, in the case of the minimum projection, also allow the visualization of the position and propagation of the transverse cracks relative to the melt pool boundary. The positions of the tip of the transverse cracks (dark areas in Fig. 5) during their propagation in the semisolid region are highlighted with a red-dashed line. The melt pool boundary at the onset of solidification is highlighted with a blue-dashed line.

Fig. 6 illustrates the minimum projection images from the aligned stack of streak images of the X-ray recordings for the different process parameters. The corresponding average intensity projections are provided in the supplementary data of this publication [13]. The purple-dotted vertical lines indicate the average x-position x_{init} (as defined in Fig. 4c) of the initiation sites of three transverse hot cracks observed in the X-ray recordings. The green-dotted vertical lines indicate the average x-position x_{stop} (as defined in Fig. 4e), at which the cracks stopped propagating. The transparent error bands span the minimum and maximum x-positions of the initiation and stop of the cracks observed for three transverse hot cracks at the same process parameter. The blue-dotted vertical lines indicate the position x_{end} at the end of the melt pool.

In Fig. 6a-d, the minimum projection images of welds produced at a welding speed of v = 30 m/min and different laser powers P are compared. For laser powers of P = 3500 W (Fig. 6a), P = 4000 W (Fig. 6b), and P = 4700 W (Fig. 6c), the transverse cracks were initiated near the end of the melt pool in approximately half of the depth of the weld seam and propagated to the surface. At a laser power of P = 5700 W (Fig. 6d), transverse hot cracks initiated at approximately two-thirds of the weld depth and two-thirds of the melt pool length and propagated in the semisolid region below the melt pool to the sample's surface.

Fig. 6d-g depicts minimum projection images of welds produced with different welding speeds v with the laser power P adjusted for a weld depth of s = 1.5 mm. At a welding speed of v = 18 m/min, the transverse cracks were initiated at a shallower depth and closer to the end of the melt pool compared to v = 30 m/min. For welding speeds of v = 12 and 6 m/min (Fig. 6f-g), transverse cracks initiated at pores formed due to capillary instabilities and propagated from these sites in the semisolid region. The determination of the positions of the cracks in the minimum images at welding speeds of v = 6 m/min and v = 12 m/min was challenging, as the edges of the pores led to dark parts in the minimum projection image, therefore altering the gray values in the area of interest. Thus, the region used for streak image processing was restricted to the area around the transverse cracks, with the width reduced from 1.5 mm to 0.5 mm for v = 12 m/min, and to 0.2 mm for v = 6 m/min. At v = 6 m/min, in contrast to higher welding speeds, some cracks stop at roughly half of the weld depth rather than reaching the sample's surface, indicating that pores act as primary initiation sites at low welding speeds.

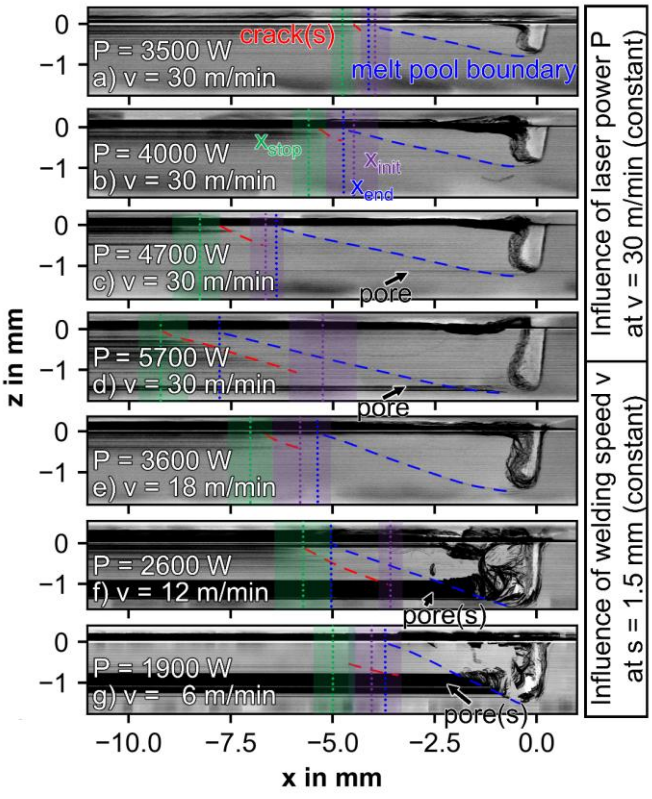


Fig. 6. Minimum image projections from processed streak images of X-ray recordings. (a-d) Welds produced at a welding speed of v = 30 m/min and different laser powers P. (d-g) Welds produced at welding speeds of v = 30 m/min (d), v = 18 m/min (e), v = 12 m/min (f), and v = 6 m/min (g), with the laser power P adjusted for a weld depth of s = 1.5 mm. Corresponding X-ray videos and projections of processed streak images are available at [13].

The distance from the melt pool boundary (blue-dashed lines in Fig. 6) perpendicular to the position of crack initiation x_{init} (purple-dotted vertical lines in Fig. 6) is similar for all investigated process parameters and ranges from approximately 350 to 550 µm. The distance between the transverse cracks and the melt pool boundary increases at lower x-positions toward the end of the melt pool. The similar slopes of the propagation path of the tips of transverse hot cracks (red-dashed lines in Fig. 6) and the melt pool boundary (blue-dashed lines in Fig. 6) in the x-z plane indicate that the crack propagation in the semisolid region follows the local solidification. This suggests that crack propagation occurs at a characteristic isotherm associated with a critical solid fraction in the semisolid region, with a slope similar to that of the liquidus isotherm at the melt pool boundary.

To further quantify this relation, the local solidification rate

$$R_{xz} = cos(\beta) \cdot v \quad (1)$$

at the melt pool boundary in the x-z-plane (blue arrow in Fig. 5b-c) was calculated from the average and minimum projection images of the streak images presented in Fig. 6, with the welding speed v and the local angle

$$\beta = tan^{-1}\left(\frac{\Delta z}{\Delta x}\right) \quad (2)$$

between the welding direction in positive x-direction and the normal to the melt pool boundary, as defined in Fig. 5b-c.

The colored lines in Fig. 7 show the local solidification rates R_{xz} at the melt pool boundary as a function of the coordinate x and the laser power P (Fig. 7a) at a welding speed of 30 m/min and as a function of the welding speed v (Fig. 7b) at a weld depth of s = 1.5 mm. The error bands span the minimum and maximum values obtained from the minimum and average image projections of the stack of streak images. The data points highlighted with a triangle correspond to the position of the initiation of the cracks x_{init}, as shown in Fig. 6. The data points highlighted with a cross correspond to the position x_{end} at the end of the melt pool (Fig. 6). The melt pool boundary at the sample's surface at $z = 0$ mm is not clearly visible in the X-ray recordings and the processed streak images. Since the solidification rate R_{xz} is expected to correspond to the welding speed v at the end of the melt pool, the values were set to $R_{xz}(x = x_{end}, z = 0\ \text{mm}) = v$. The solidification rates R_{xz} equal 0 mm/s at the bottom of the melt pool at the onset of solidification. Despite varying laser powers P at a constant welding speed of v = 30 m/min, the solidification rates R_{xz} (Fig. 7a) in the central part of the melt pool in the x-z plane remain approximately constant at 100 to 110 mm/s. Differences only arise from the varying lengths of the melt pools. The solidification rates $R_{xz,}$ for welds with different welding speeds v at a weld depth of s = 1.5 mm (Fig. 7b), also remain constant over a large central part of the melt pool with an increasing magnitude for increasing welding speeds.

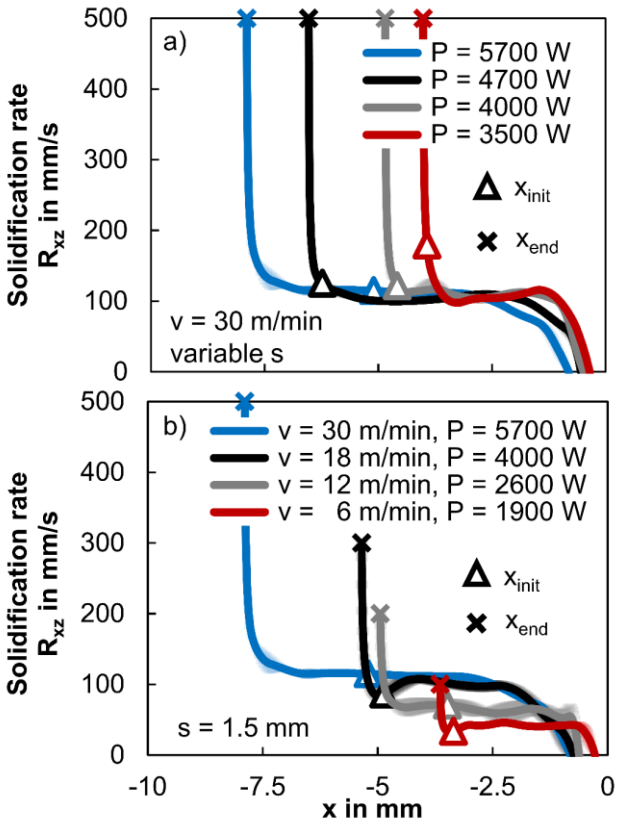


Fig. 7. Solidification rate R_{xz} as a function of the coordinate x at a welding speed of v =30 m/min and different laser powers P (a) and at different welding speeds v and a weld depth of s = 1.5 mm (b).

At welding speeds above v = 18 m/min, the solidification rates R_{xz} in the central part of the melt pool tend to saturate at approximately 100 mm/s.

The average solidification rate $R_{c,xz}$ at the melt pool boundary encountered during crack propagation was calculated to investigate the influence on the crack propagation. The position of the stop of the crack x_{stop} lies at lower x-positions than the end of the melt pool x_{end} (Fig. 6). The average solidification rate $R_{c,xz}$ at the melt pool boundary was therefore determined from the average values of the solidification rate between x_{init} (triangles in Fig. 7) and x_{end} (crosses in Fig. 7).

The average solidification rates $R_{c,xy}$ encountered during crack propagation and the average crack propagation rate $v_{c,xz,}$ in the x-z plane are shown in Fig. 8. The average crack propagation rate

$$v_{c,xz} = \frac{\Delta l_{c,xz}}{t_{stop} - t_{init}} \quad (3)$$

was calculated as the ratio between the propagation length $\Delta l_{c,xz}$ of the cracks in the x-z plane (as defined in Fig. 4e) and the propagation time t_{stop}-t_{init} (Fig. 4c-e). For each set of process parameters, three transverse cracks were analyzed.

The trend in Fig. 8a shows that the crack propagation rate decreases with increasing laser power P at a constant welding speed of v = 30 m/min.

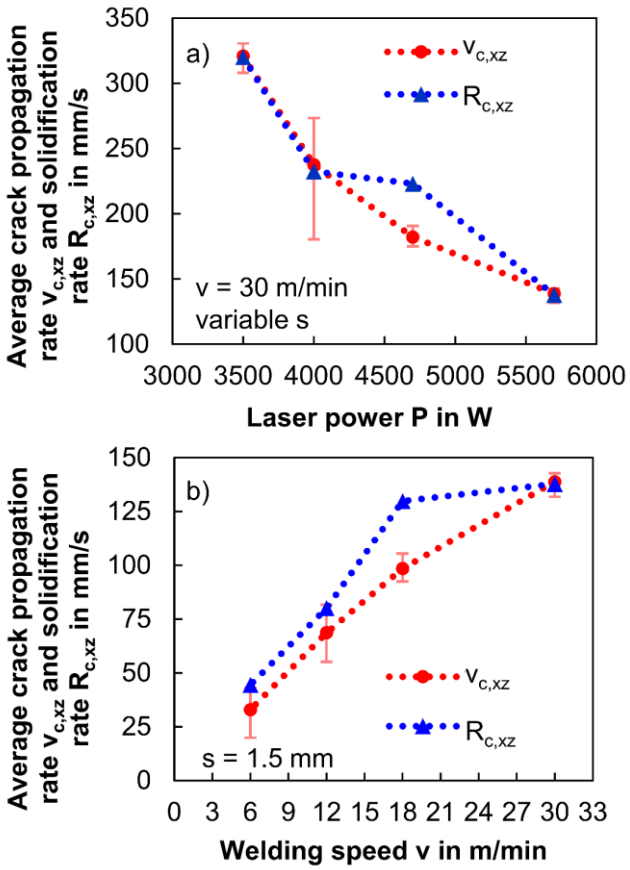


Fig. 8. Average crack propagation rate $v_{c,xz}$ (red circles) and average solidification rate $R_{c,xy}$ (blue triangles) at the melt pool boundary during crack propagation as a function of the laser power P at a welding speed of v =30 m/min (a) and the welding speed v at a weld depth of s = 1.5 mm (b).

This is a result of the positions of crack initiation relative to the melt pool boundary. At lower laser powers, cracks were initiated near the end of the melt pool, where local solidification rates are higher than in the central area (Fig. 7a). This observation matches the findings of an initiation with high crack propagation rates at the end of the melt pool in laser additive manufacturing [9, 10].

For the highest investigated laser power of P = 5700 W, the cracks were already initiated in the central part of the melt pool (Fig. 6), with lower solidification rates resulting in a lower average crack propagation rate. A clear increase in the average crack propagation rate with increasing welding speed at a weld depth of s = 1.5 mm can be observed in Fig. 8b. This trend results from the higher solidification rates R_{xz} at the melt pool boundary during crack propagation at higher welding speeds.

The average crack propagation rate closely matches the average solidification rate at the melt pool boundary in the *x*-*z* plane encountered during crack propagation. This correlation is observed across a wide range of process parameters, including variation of both laser power and welding speed, and therefore indicates a strong connection between the propagation of transverse hot cracks and local solidification.

5. Conclusion

In-situ X-ray imaging of transverse hot crack formation revealed that the process parameters influence the number of transverse hot cracks in the weld seam as well as the local solidification conditions. The solidification conditions govern both the position where cracks initiate relative to the melt pool boundary as well as the average crack propagation rate. The average crack propagation rate closely corresponds to the local solidification rate in the *x*-*z* plane encountered during crack propagation. At welding speeds below 12 m/min, fewer cracks, mainly initiated at pores with lower crack propagation rates, were observed. At a higher welding speed of 30 m/min, more cracks were initiated near the end of the melt pool at lower laser powers, and in the semisolid region below the melt pool at higher laser powers. Higher crack propagation rates were observed for these cracks compared to those observed at lower welding speeds. These findings provide a basis for strategies to mitigate transverse hot cracking. At low welding speeds, reducing pores is essential to reduce crack initiation sites. At higher welding speeds, mitigation requires optimized conditions at the identified locations of the initiation of transverse hot cracks. The observed relationship between crack propagation rate and local solidification rate may provide a basis for approaches to control or mitigate crack growth through targeted adjustment of local solidification conditions by means of dynamic beam shaping.

Acknowledgements

This work was funded by the Deutsche Forschungsgemeinschaft (DFG, German Research Foundation) – 558591047. The presented investigations were carried out within the cooperation “Laser Meets Synchrotron” (www.laser-meets-synchrotron.de). The experimental setup and its operation were funded by the Deutsche Forschungsgemeinschaft e.V. (DFG, German Research Foundation) within the framework of the Collaborative Research Centre SFB1120-236616214 “Bauteilpräzision durch Beherrschung von Schmelze und Erstarrung in Produktionsprozessen”. We acknowledge Hereon (Geesthacht, Germany) and DESY (Hamburg, Germany), members of the Helmholtz Association HGF, for the provision of experimental facilities. The experiments were carried out at Beamline P07 of PETRA III as part of proposal BAG-20211050 and we would like to thank F. Beckmann, J. Moosmann and all people involved for their support.

Appendix A. Supplementary data

The supplementary data to this publication contains the X-ray recordings and the processed streak images. https://doi.org/10.18419/DARUS-5782 [13].

References

[1] Michel, J., Wagner, J., Holder, F., Zaiß, F. *et al.* Mechanisms of transverse hot crack formation during laser welding of high-strength aluminum alloys at high welding speeds. Optics & Laser Technology 2025; 192, p. 113898.

[2] Hu, B., Richardson, I.M. Mechanism and possible solution for transverse solidification cracking in laser welding of high strength aluminium alloys. Materials Science and Engineering A, Structural Materials: Properties, Microstructure and Processing 2006; 429, p. 287–294.
[3] Hagenlocher, C., Fetzer, F., Weber, R., Graf, T. Benefits of very high feed rates for laser beam welding of AlMgSi aluminum alloys. Journal of Laser Applications 2018; 30.
[4] Rappaz, M., Drezet, J.-M., Gremaud, M. A new hot-tearing criterion. Metallurgical and Materials Transactions A 1999; 30, p. 449–455.
[5] Michel, J., Bachmann, M., Yu, P.-H., Riedmüller, K.R. *et al.* Reduction of transverse hot cracking in laser welds of aluminium sheets by residual compressive stresses induced by forming of near-surface embossings. IOP Conference Series: Materials Science and Engineering 2025; 1332, p. 12011.
[6] Forster, C., Döring, M., Spurk, C., Hummel, M. *et al.* In-situ observation of end crater crack mechanisms in AA7075 during laser beam welding using synchrotron radiation. Procedia CIRP 2024; 124, p. 464–467.
[7] Seibold, M., Schricker, K., Schmidt, L., Diegel, D. *et al.* Temporal and spatial determination of solidification rate during pulsed laser beam welding of hot-crack susceptible aluminum alloys by means of high-speed synchrotron X-ray imaging. Journal of Advanced Joining Processes 2024; 10, p. 100235.
[8] Chen, Y., Zhang, D., O'Toole, P., Qiu, D. *et al.* In situ observation and reduction of hot-cracks in laser additive manufacturing. Communications Materials 2024; 5.
[9] Kouraytem, N., Chiang, P.-J., Jiang, R., Kantzos, C. *et al.* Solidification crack propagation and morphology dependence on processing parameters in AA6061 from ultra-high-speed x-ray visualization. Additive Manufacturing 2021; 42, p. 101959.
[10] Rees, D.T., Leung, C.L.A., Elambasseril, J., Marussi, S. *et al.* In situ X-ray imaging of hot cracking and porosity during LPBF of Al-2139 with TiB2 additions and varied process parameters. Materials & Design 2023; 231, p. 112031.
[11] Schell, N., King, A., Beckmann, F., Fischer, T. *et al.* The High Energy Materials Science Beamline (HEMS) at PETRA III. Materials Science Forum 2013; 772, p. 57–61.
[12] Novelis Advanz 6HS-s650. https://de.novelis.com/product/novelis-advanz-6hs-s650/. Accessed 14 July 2022.
[13] Michel, J., Supplementary Data for Paper "Synchrotron X-ray imaging of the formation of transverse hot cracks during laser welding of a high-strength aluminum alloy and their dependence on local solidification conditions and process parameters", 2026. doi: 10.18419/DARUS-5782.